This article was downloaded by: *[Ling, F.]*
On: *8 October 2010*
Access details: *Access Details: [subscription number 927492908]*
Publisher *Taylor & Francis*
Informa Ltd Registered in England and Wales Registered Number: 1072954 Registered office: Mortimer House, 37-41 Mortimer Street, London W1T 3JH, UK

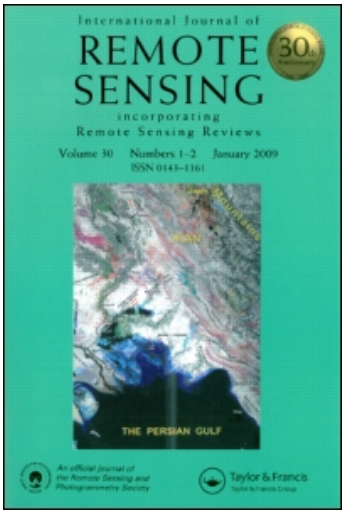

International Journal of Remote Sensing
Publication details, including instructions for authors and subscription information:
http://www.informaworld.com/smpp/title~content=t713722504

Super-resolution land-cover mapping using multiple sub-pixel shifted remotely sensed images

Feng Ling[a]; Yun Du[a]; Fei Xiao[a]; Huaiping Xue[a]; Shengjun Wu[a]
[a] Institute of Geodesy and Geophysics, Chinese Academy of Sciences, Wuhan, PR China

Online publication date: 01 October 2010

To cite this Article Ling, Feng , Du, Yun , Xiao, Fei , Xue, Huaiping and Wu, Shengjun(2010) 'Super-resolution land-cover mapping using multiple sub-pixel shifted remotely sensed images', International Journal of Remote Sensing, 31: 19, 5023 — 5040
To link to this Article: DOI: 10.1080/01431160903252350
URL: http://dx.doi.org/10.1080/01431160903252350

PLEASE SCROLL DOWN FOR ARTICLE

Full terms and conditions of use: http://www.informaworld.com/terms-and-conditions-of-access.pdf

This article may be used for research, teaching and private study purposes. Any substantial or systematic reproduction, re-distribution, re-selling, loan or sub-licensing, systematic supply or distribution in any form to anyone is expressly forbidden.

The publisher does not give any warranty express or implied or make any representation that the contents will be complete or accurate or up to date. The accuracy of any instructions, formulae and drug doses should be independently verified with primary sources. The publisher shall not be liable for any loss, actions, claims, proceedings, demand or costs or damages whatsoever or howsoever caused arising directly or indirectly in connection with or arising out of the use of this material.

International Journal of Remote Sensing
Vol. 31, No. 19, 10 September 2010, 5023–5040

Taylor & Francis
Taylor & Francis Group

Super-resolution land-cover mapping using multiple sub-pixel shifted remotely sensed images

FENG LING*, YUN DU, FEI XIAO, HUAIPING XUE and SHENGJUN WU
Institute of Geodesy and Geophysics, Chinese Academy of Sciences, No 340, Xudong Road, Wuhan, PR China

(*Received 31 July 2008; in final form 26 January 2009*)

Downloaded By: [Ling, F.] At: 01:31 8 October 2010

Super-resolution land-cover mapping is a promising technology for prediction of the spatial distribution of each land-cover class at the sub-pixel scale. This distribution is often determined based on the principle of spatial dependence and from land-cover fraction images derived with soft classification technology. However, the resulting super-resolution land-cover maps often have uncertainty as no information about sub-pixel land-cover patterns within the low-resolution pixels is used in the model. Accuracy can be improved by incorporating supplemental datasets to provide more land-cover information at the sub-pixel scale; but the effectiveness of this is limited by the availability and quality of these additional datasets. In this paper, a novel super-resolution land-cover mapping technology is proposed, which uses multiple sub-pixel shifted remotely sensed images taken by observation satellites. These satellites take images over the same area once every several days, but the images are not identical because of slight orbit translations. Low-resolution pixels in these remotely sensed images therefore contain different land-cover fractions that can provide useful information for super-resolution land-cover mapping. We have constructed a Hopfield Neural Network (HNN) model to solve it. Maximum spatial dependence is the goal of the proposed model, and the fraction maps of all images are constraints added to the energy function of HNN. The model was applied to synthetic artificial images as well as to a real degraded QuickBird image. The output maps derived from different numbers of images at different zoom factors were compared visually and quantitatively to the super-resolution map generated from a single image. The resulting land-cover maps with multiple remotely sensed images were more accurate than was the single image map. The use of multiple remotely sensed images is therefore a promising method for decreasing the uncertainty of super-resolution land-cover mapping. Moreover, remotely sensed images with similar spatial resolution from different satellite platforms can be used together, allowing a fusion of information obtained from remotely sensed imagery.

1. Introduction

Information regarding the extent of land cover is important in many scientific research fields such as ecology, agriculture and hydrology. Many types of land-cover information for these applications are now provided by remote sensing technology, due to its outstanding performance (Bonnett and Campbell 2002). At present, a number of satellite sensors are routinely used to provide remotely sensed imagery with

*Corresponding author. Email: lingf@asch.whigg.ac.cn

International Journal of Remote Sensing
ISSN 0143-1161 print/ISSN 1366-5901 online © 2010 Taylor & Francis
http://www.tandf.co.uk/journals
DOI: 10.1080/01431160903252350

different spatial resolution for scientific research studies (Loveland *et al.* 2000, Song *et al.* 2001, Friedl *et al.* 2002, Sawaya *et al.* 2003). These include Advanced Very High Resolution Radiometer (AVHRR) with a spatial resolution of about 1000 m, Moderate Resolution Imaging Spectroradiometer (MODIS) with spatial resolutions of 250 m, 500 m or 1000 m, Advanced Spaceborne Thermal Emission and Reflection Radiometer (ASTER) with spatial resolutions of 90 m, 30 m or 15 m, Landsat Thematic Mapper (TM) with a spatial resolution of 30 m, and QuickBird with 2.4 m multispectral and 0.6 m panchromatic imagery. Images from these sources can provide land-cover information at spatial resolutions that are suitable for research ranging from the global scale to the local scale.

Extraction of land-cover information from remotely sensed imagery is often accomplished with classification technologies. However, imagery classification is always a difficult task and the characteristics of the resulting land-cover maps derived from different images are not always the same (Bonnett and Campbell 2002). Moreover, when the sensor's instantaneous field-of-view (IFOV) includes more than one land-cover class on the ground, there are mixed pixels in the remotely sensed imagery. Because their spectral characteristics are not representative of any single land-cover class, mixed pixels present one of the most difficult problems in the derivation of land-cover information from remotely sensed images (Fisher 1997, Cracknell 1998). With hard classification methods, each pixel in an image is considered to be a unit belonging to a single land-cover class. Mixed pixels are assigned to the class with the highest proportion of coverage, with the result that the land-cover map produced is inaccurate. Although the use of remotely sensed imagery with high spatial resolution can provide a better understanding of land-cover information by decreasing the phenomenon of mixed pixels, usage of this type of technology is limited by a number of factors, such as its temporal resolution, its spectral resolution and the high costs associated with it.

One alternative method for addressing the problem of mixed pixels in remotely sensed imagery is soft classification technology (Foody 1996, Liu and Wu 2005). In contrast to hard classification technologies, soft classification approaches do not assign mixed pixels as a single land-cover class but instead predict the proportional cover of each land-cover class within each mixed pixel. Soft classification approaches that have been proposed include linear spectral mixture modelling (Holben and Shimabukuro 1993, GarciaHaro *et al.* 1996), fuzzy c-means classifiers (Atkinson *et al.* 1997, Bastin 1997), artificial neural networks (Carpenter *et al.* 1999, Foody 2002, Liu *et al.* 2004, Lee and Lathrop 2006), regression trees (Liu and Wu 2005), expert system rules (Hung and Ridd 2002) and support vector machines (Brown *et al.* 2000). However, although soft classification can provide more useful land-cover information than hard classification, it can only achieve the area proportion of each class. The actual spatial distribution of each class in these mixed pixels is not distinguished by these methods (Atkinson 1997, Foody 1998, Tatem *et al.* 2001a,b).

To predict the spatial land-cover distribution within mixed pixels, super-resolution mapping, as also known as sub-pixel sharpening or sub-pixel mapping, is proving to be a promising method. First introduced by Atkinson (1997), this type of land-cover mapping can be considered as the post processing of soft classification. Thus, super-resolution mapping techniques take the fraction values yielded by soft classification and use these as input to retrieve an appropriate spatial location for specific land-cover fractions. Current super-resolution mapping methods include the Hopfield neural network (HNN) (Tatem *et al.* 2001a,b, 2002, 2003), linear optimization (Verhoeye and

Downloaded By: [Ling, F.] At: 01:31 8 October 2010

De Wulf 2002), genetic algorithm (Mertens *et al.* 2003), feed-forward neural network (Mertens *et al.* 2004), Markov random field (Kasetkasem *et al.* 2005), pixel swapping (Atkinson 2005, Thornton *et al.* 2007) and simulated annealing (Makido *et al.* 2007).

In general, super-resolution mapping can be formulated as an inverse problem that reconstructs a fine spatial resolution map of land-cover class labels from a set of class fractions provided by a low-resolution image. However, the inverse problem is underdetermined and different fine resolution land-cover class maps can each lead to equally possible, but different, reproductions of the available low-resolution fractions (Nguyen *et al.* 2006). Therefore, there is always uncertainty caused by super-resolution mapping due to the lack of information about sub-pixel land-cover pattern. Additional site-specific land-cover information at the sub-pixel scale would be useful in decreasing the uncertainty.

This type of additional information for super-resolution mapping issues is available in a number of different datasets, such as the panchromatic band images (Foody 1998, Nguyen *et al.* 2006), vector boundaries (Aplin and Atkinson 2001), light detection and ranging (Lidar) data (Nguyen *et al.* 2005) and digital elevation model (DEM) (Ling *et al.* 2008). In addition, prior spatial land-cover structure information, such as special patterns of linear land-cover features (Thornton *et al.* 2007), class labels at a set of fine pixels (Boucher and Kyriakidis 2007) or the structural information encapsulated in a set of indicator variogram models (Tatem *et al.* 2002, Atkinson *et al.* 2008, Robin *et al.* 2008), also can be successfully applied to improve the accuracy of super-resolution mapping. However, these methods still have their own limitations, largely arising from the accessibility of ancillary datasets. In most cases, accurate ancillary datasets are unavailable, which immediately hampers the usability of these methods. Second, incorporation of ancillary datasets will bring about additional uncertainty, and the resulting map accuracy will also be affected by the dataset quality. Lastly, these methods are often designed for special situations. For instance, the method of using high-resolution DEM to improve waterline mapping is based on the feature of water flow, and is therefore unsuitable for land-cover classes other than waterlines (Ling *et al.* 2008).

In light of these limitations and issues, this paper proposes the examination of an undervalued source of additional data for super-resolution mapping. It is well known that satellite remote sensing has a multiobservation capability; that is, the observation satellite takes images over the same area of land surface once every several days as it orbits around the Earth. These observed images are always not identical to each other, even under the same weather conditions, because of the slight orbit-translation caused by orbit swing (Lu and Inamura 2003). Consequently, the pixels in remotely sensed images acquired at different times are shifted at the sub-pixel scale, such that each pixel contains different land-cover classes. Fraction maps derived from these images can therefore provide additional land-cover information at the sub-pixel scale, which can theoretically be used to improve the accuracy of super-resolution mapping. The main objective of this paper is to investigate the potential of these multiple sub-pixel shifted images as a means of improving the accuracy of super-resolution land-cover mapping.

2. Methodology

2.1 *Super-resolution mapping with a single image and its uncertainty*

The aim of super-resolution mapping is to predict the most suitable locations for the different class fractions within each low-resolution pixel (Atkinson 1997). In general, each low-resolution pixel was first divided into a pre-defined number of sub-pixels.

Downloaded By: [Ling, F.] At: 01:31 8 October 2010

The number of sub-pixels of every class within each low-resolution pixel was then assigned according to the fraction values. Finally, the spatial distribution of these sub-pixels was determined based on the principle of spatial dependence (Mertens *et al.* 2003). The most important hypothesis of super-resolution mapping is the spatial correlation of natural phenomena; i.e. the tendency that, for a given property, spatially proximate observations are more alike than more distant observations. Although this principle has been proven to be acceptable (Atkinson 1997), super-resolution mapping with a single image (SMSI) always has uncertainty, as fraction maps derived from only one image cannot provide sufficient information about the land-cover distribution at the sub-pixel scale.

A simple representation of SMSI is given in figure 1 (adapted from Nguyen *et al.* 2006). The sample is a raster grid of 3×3 low spatial resolution pixels with two land-cover classes, shown as white and black. Numbers in these pixels are the associated proportions of the first land-cover class (figure 1(*a*)). Three possible spatial configurations of land-cover at the sub-pixel scale are represented in figures 1(*b*)–(*d*). All of these land-cover pattern maps satisfy the fraction map shown in figure 1(*a*), but the spatial distribution of sub-pixels in the central pixel is much different. Focusing first on figures 1(*b*) and (*c*), the spatial sub-pixel distribution shown in figure 1(*c*) has a higher spatial dependence than that seen in figure 1(*b*). Based on the assumption of maximum spatial dependence, the land-cover spatial pattern shown in figure 1(*c*) is believed to be more accurate than that shown in figure 1(*b*); thus, the result of super-resolution mapping is figure 1(*c*). However, when we compare figures 1(*c*) and (*d*), both land-cover patterns are seen to have the same spatial dependence and it is not possible to determine which is the final solution of super-resolution mapping. Thus, the spatial land-cover distribution at the sub-pixel scale cannot be precisely predicted using only fraction maps derived from one image and the spatial dependence principle.

Downloaded By: [Ling, F.] At: 01:31 8 October 2010

2.2 *Super-resolution reconstruction with multiple images*

The concept of 'super-resolution' has been widely used in digital image processing since Tsai and Huang (1984) first introduced a frequency analysis model for super-resolution reconstruction of a globally translated image sequence. In contrast to the concept of 'super-resolution mapping', this 'super-resolution reconstruction' concept refers to the construction of a single high-resolution image from multiple aligned low-resolution images that have sub-pixel shifts. 'Super-resolution mapping', on the

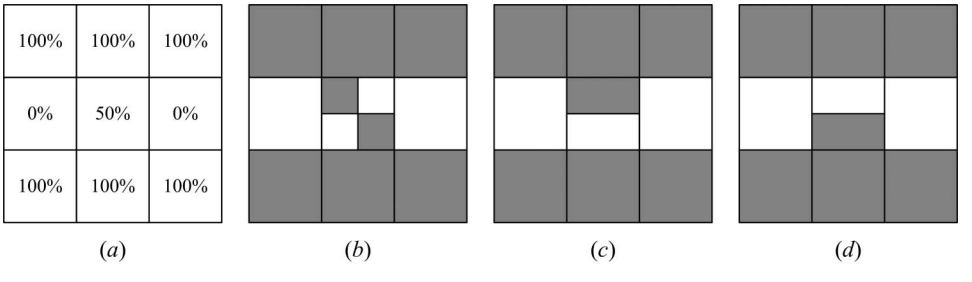

Figure 1. Spatial dependence principle of super-resolution land-cover mapping and its uncertainty. (*a*) Land cover proportion raster grid of 3×3 low-resolution pixels. (*b*) Possible super-resolution mapping result without maximal spatial dependence. (*c*) and (*d*) Two possible super-resolution mapping results based on maximizing spatial dependence. Adapted from Nguyen *et al.* (2006), with permission.

other hand, means the construction of final land-cover maps from the soft classification result of a single image.

The basic idea behind super-resolution reconstruction is the combination of several low-resolution images from the same scene to produce one or several images with a higher resolution. In general, the low spatial resolution images represent different 'looks' at the same scene. In most situations, these images are not absolutely overlapped and there are different sub-pixel shifts between them. Because of this, none of these low-resolution images is exactly the same as the others because each image contains a certain amount of different information from the same scene. Therefore, the different information contained in each low spatial resolution image can be exploited to recover a high spatial resolution image (Park *et al.* 2003, Choi *et al.* 2004).

Due to its importance and usefulness, super-resolution reconstruction technology has become one of the most active fields for image processing researchers and has achieved successful applications in many fields. Many super-resolution reconstruction algorithms have been proposed, including Iterative Backward Projection (IBP) (Irani and Peleg 1991), frequency domain processing (Kim and Su 1993), Projection Onto Convex Sets (POCS) (Stark and Oskoui 1989), the maximum *a posteriori* (MAP) approach (Hardie *et al.* 1997) and adaptive filtering (Elad and Feuer 1999). Several well-cited documents can be accessed for a more complete review of super-resolution construction of images (Sean and Robert 1998, Park *et al.* 2003).

Super-resolution reconstruction technology has also been applied to remotely sensed imagery. Maltamo *et al.*(2003) combined several high-resolution video images in order to improve the ability to distinguish single trees. Lu and Inamura (2003) compared several existing super-resolution reconstruction algorithms and presented a practical implementation based on the IBP algorithm. Their experimental results showed that this algorithm can achieve a highly improved resolution image from its low-resolution image sequences. Packalen *et al.* (2006) analysed the ability to recognize forested and non-forested areas from multiple AVHRR images and showed that it was difficult to identify a significant quantitative improvement, although the super-resolution technique seemed to be successful visually.

This previous research showed that super-resolution reconstruction technology can provide better visual results than those based on the original image. However, there are also some disadvantages of using a time-series of satellite images in super-resolution image production. First, the multiple remotely sensed images captured on different days are often obtained under different weather conditions. Since it is difficult to eliminate the effect of atmosphere on these satellite images, these images are hard to be fused. Second, super-resolution reconstruction technology often leads to spectral distortion. As the final object of using remotely sensed imagery is often the extraction of land-cover information or object recognition, spectral distortion will increase uncertainty of the result and generate more artefacts. Lastly, super-resolution reconstruction technology is only suitable for images obtained from the same satellite sensors. As the imaging model and the spectral band are very different, remotely sensed images from different platforms, such as TM and ASTER, AVHRR and MODIS, cannot be fused to provide super-resolution land-cover information.

2.3 *Super-resolution mapping with multiple sub-pixel shifted images*

Super-resolution methods fuse multiple low-resolution images to first construct a single high-resolution image, and then use the resulting high-resolution image to

Downloaded By: [Ling, F.] At: 01:31 8 October 2010

extract land-cover information with classification technologies. In the current study, we propose an approach of super-resolution mapping with multiple sub-pixel shifted images (SMMI). In this method, all low-resolution remotely sensed images are first classified with a soft classification method to acquire fraction images. All of the derived fraction images are then considered as inputs of super-resolution mapping for extraction of the high-resolution land-cover map. The fundamental principle of 'super-resolution reconstruction' is still used in the proposed SMMI technology; that is, if the low-resolution images have different sub-pixel shifts from each other, different land-cover information at the sub-pixel scale contained in each low-resolution image is exploited to obtain a high-resolution land-cover map.

Three simple examples shown in figure 2 are used to illustrate the proposed SMMI technology. The illustration is an extension of the example discussed in section 2.1 (figure 1). If we have the image shown in figure 1(*a*) and also another sub-pixel shifted image, both images can be used for SMMI.

In the first example, the additional image shown in figure 2(*a*) is a land-cover proportion raster image of 3×3 low-resolution pixels. For simplicity, the coarse resolution pixel was split into 2×2 sub-pixels. If the shift between both images is known (it is set to be 0.5 pixel in this example), figure 1(*a*) (with a letter 'F' in the left bottom corner) and figure 2(*a*) can be overlapped exactly and the result is shown in figure 2(*b*). The resulting map of SMMI is shown in figure 2(*c*), whose sub-pixel raster corresponds with figure 1(*a*). As mentioned above, when only a single image is available, super-resolution mapping result often has uncertainty. With two overlapped images, the uncertainty can be eliminated and the result shown in figure 2(*c*) becomes the only solution, because no other sub-pixel distributions can simultaneously satisfy these two fraction images.

The second example is shown in figures 2(*d*), 2(*e*) and 2(*f*). In this case, the additional image is different from the first one. Figure 2(*f*) shows the result of SMMI with two overlapped images shown as figure 2(*e*). In this situation, the spatial land-cover patterns that have maximum spatial dependence, such as figures 1(*c*) and 1(*d*), cannot be considered as possible solutions any longer as their land-cover proportions no longer simultaneously satisfy both fraction maps. The resulting map shown in figure 2(*f*) is the solution, even though it lacks maximum spatial dependence.

The third example shown in figures 2(*g*), 2(*h*) and 2(*i*) is used to illustrate the SMMI technology when multiple images have different spatial resolutions. In this example, a 2×2 pixel image with a coarser spatial resolution (1.5 times as the first image) was used. Each pixel in figure 2(*g*) is split into a 3×3 sub-pixel raster to make the spatial resolution of sub-pixels the same as that in figure 1(*a*). With the overlapped images shown in figure 2(*h*), the resulting map shown in figure 2(*i*) can also be exactly extracted, as no other land-cover pattern can satisfy both fraction maps.

Compared with one single remotely sensed image, multiple remotely sensed images with sub-pixel shifts contain more useful land-cover information, as seen in the example shown above. Incorporating this information into the super-resolution mapping procedure can therefore improve the accuracy of the resulting high-resolution land-cover map.

Compared with the 'super-resolution reconstruction first and then classification' technology, the proposed method has several specific advantages. First, the input of the proposed method is not the reflected value of the images but rather is the soft classification fraction maps extracted individually from each image. For the former super-resolution reconstruction method, different atmospheric conditions will greatly

Downloaded By: [Ling, F.] At: 01:31 8 October 2010

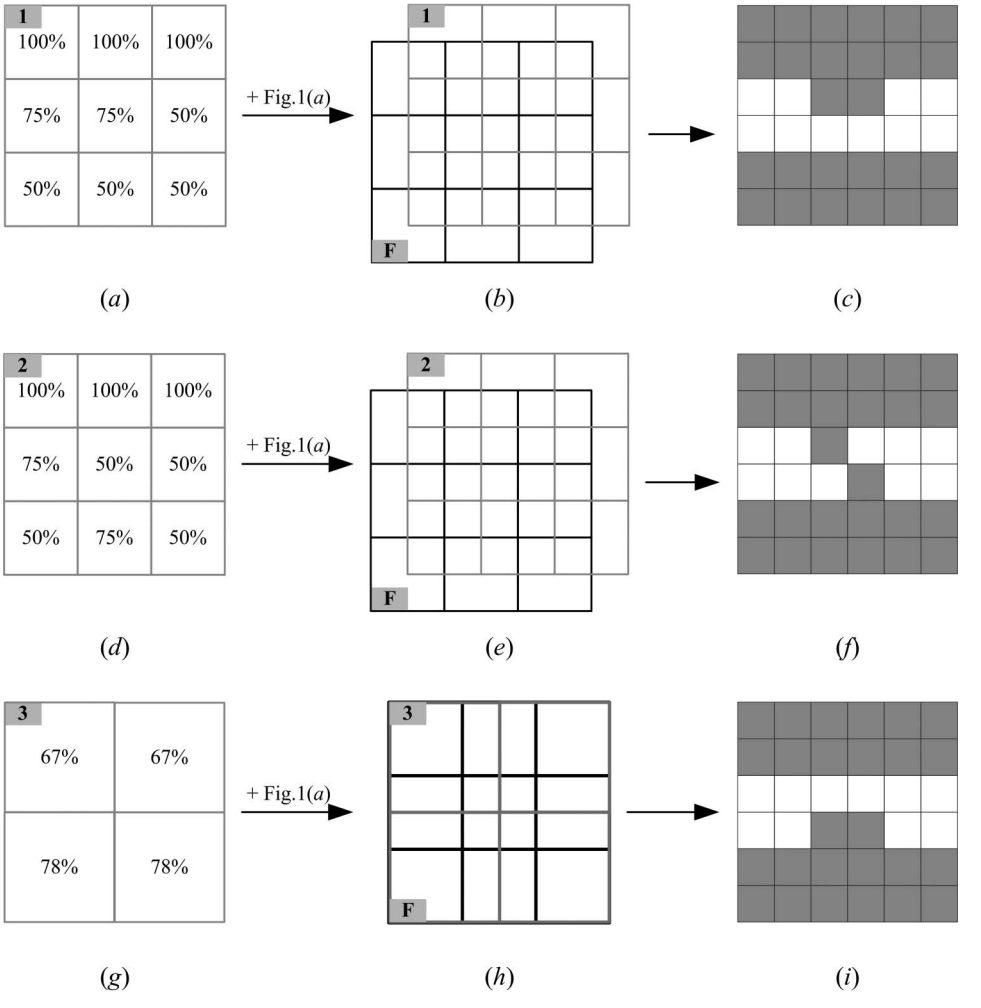

Figure 2. SMMI with different additional images. (*a*), (*d*) and (*g*) Three different land cover proportion raster grids. (*b*), (*e*) and (*h*) Overlapping results of (*a*), (*d*) and (*g*) with the image shown in figure 1(*a*) (with 'F' in the left bottom corner). (*c*), (*f*) and (*i*) Resulting maps at the sub-pixel scale, derived with the multiple images shown in (*b*), (*e*) and (*h*).

affect the results. Thus, atmosphere correction, a complex and difficult task, must first be performed. In the proposed method, however, the pixels are initially unmixed. Images are dealt with individually and the different atmospheric conditions should not affect analysis. For most situations, the atmospheric correction procedures can be ignored as the atmosphere conditions are often similar in a regional area in each individual image. Second, the former super-resolution reconstruction technology can only be used for images acquired by the same sensor. With the proposed method, remotely sensed images from different platforms can readily be fused to reconstruct the resulting high-resolution land-cover map, because input is not the images themselves. Moreover, even if these images do not have the same spatial resolution, they still can be fused. Thus, different images such as AVHRR and MODIS can be used

Downloaded By: [Ling, F.] At: 01:31 8 October 2010

together to provide land-cover information at the sub-pixel scale, which is a substantial improvement for remotely sensed imagery fusion.

2.4 *Hopfield neural network model for SMMI*

The Hopfield Neural Network (HNN), which has been widely used for SMSI, is used to address the problem of SMMI. The HNN model presented in this research is based on the structure of the HNN proposed by Tatem *et al.* (2001b). As the model has been described in detail in the previous literature, it is only simply presented here. More in-depth information about the model can be accessed in a number of recent papers (Tatem *et al.* 2001a,b, 2002, 2003, Nguyen *et al.* 2005, Nguyen *et al.* 2006).

The structure of the HNN model for SMMI is illustrated in figure 3. In this example, four low-resolution images were used. Each image contains 2×2 pixels with sub-pixel shifts shown in figure 3(*a*). For super-resolution mapping, each low-resolution pixel is divided into a 5×5 interconnected matrices of neurons shown as figure 3(*b*), where the sub-pixel raster corresponds with the No.1 image. Each matrix of neurons represents a land-cover class and each neuron (k,i,j) represents a sub-pixel at position (i,j) in the land-cover class k. For SMMI, the sub-pixels not only belong to a single low-resolution image but to all low-resolution images at the same time. All fraction images derived from all images are land-cover proportion constraints of HNN. For example, the black sub-pixel in the 5th row and the 6th column (abbreviated as (r5, c6)) shown in figure 3(*b*) simultaneously corresponds with the (r1, c2) low-resolution pixel of the No.1 image, the (r2, c1) pixel of the No.2 image, the (r1, c2) pixel of the No.3 image, and the (r1, c1) pixel of the No.4 image.

The HNN is a recurrent neural network and runs until it converges to a stable state. At the stable state, the value of the energy function of the HNN is at a minimum while the spatial correlation of the sub-pixels is maximized. The output values of the neurons are binary values at the stable state. If the output value of the neuron is 1, the sub-pixel is assigned to that land-cover class. Otherwise, if the output value is 0, the sub-pixel does not belong to that class (Tatem *et al.* 2001a).

Downloaded By: [Ling, F.] At: 01:31 8 October 2010

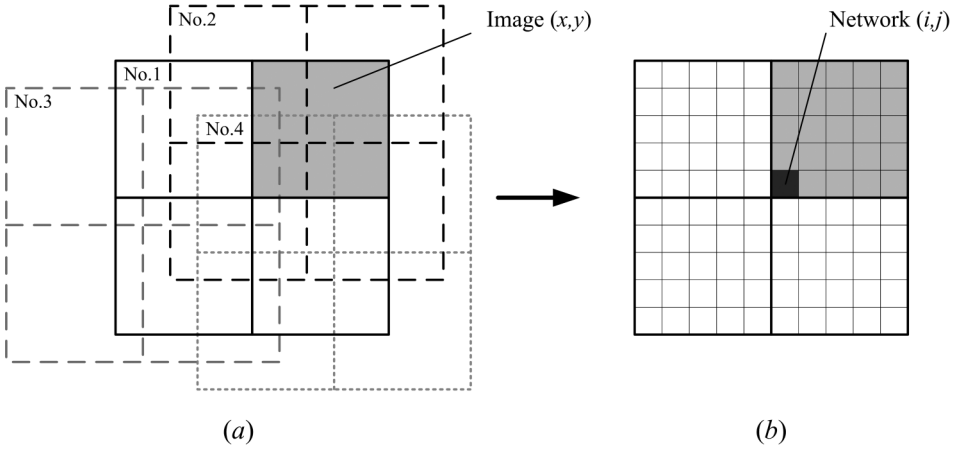

Figure 3. (*a*) Four images of 2×2 pixels with sub-pixel shifts; x and y represent the image pixel coordinates. (*b*) Representation of the Hopfield network layer; i and j represent the neuron coordinates.

The network is simulated via its equation of motion, using the Euler method:

$$\mu_{ij}(t + \mathrm{d}t) = \mu_{ij} + \frac{\mathrm{d}\mu_{ij}(t)}{\mathrm{d}t}\mathrm{d}t, \tag{1}$$

$$\frac{\mathrm{d}u_i}{\mathrm{d}t} = -\frac{\delta E}{\delta v_i}, \tag{2}$$

where $\mathrm{d}t$ is the time step of the iterative method, and the function $(\mathrm{d}u_{ij}(t)/\mathrm{d}t)$ is measured using $(\mathrm{d}E_{ij} / \mathrm{d}v)$ determined using the goals and constraints of the task.

For SMMI, the network energy function is defined as:

$$E = -\sum_k \sum_i \sum_j (W_1 C_{kij} + W_2 P_{kij} + W_3 M_{kij}), \tag{3}$$

where (k,i,j) represents a neuron at position (i,j) in the land-cover class k, C_{kij} refers to the spatial clustering function, P_{kij} is the land-cover proportion constraint and M_{kij} is the multiclass constraint value. W_1, W_2 and W_3 are values of the weighting constants, which define the effects of the corresponding goal function, proportion constraint and multiclass constraint to the energy function, respectively.

The value of the spatial clustering is the goal function of HNN. The object of this function is to make the output of a neuron similar to that of its neighbouring neurons, which is a method of achieving spatial dependence. It includes two values of $C1_{kij}$ and $C2_{kij}$ that are determined by the following equations:

$$\frac{\mathrm{d}C1_{kij}}{\mathrm{d}v_{kij}} = \frac{1}{2}\left(1 + \tanh\left(\frac{1}{8}\sum_{\substack{b=i-1 \\ b\neq i}}^{i+1}\sum_{\substack{c=j-1 \\ c\neq j}}^{j+1} v_{kbc} - 0.5\right)\lambda\right) \times (v_{kij} - 1), \tag{4}$$

$$\frac{\mathrm{d}C2_{kij}}{\mathrm{d}v_{kij}} = \frac{1}{2}\left(1 + \left(-\tanh\left(\frac{1}{8}\sum_{\substack{b=i-1 \\ k\neq i}}^{i+1}\sum_{\substack{c=j-1 \\ k\neq j}}^{j+1} v_{kbc}\right)\lambda\right)\right) \times (v_{kij}), \tag{5}$$

where λ is the gain or the steepness of the tanh function, 0.5 is the threshold and v_{kij} is the output value of the neuron (k,i,j). The first function (4) aims to increase the output value v_{kij} of the centre neuron to 1 if the average output of the surrounding eight neurons is greater than 0.5. The second function (5) aims to decrease the output for each layer of the centre neuron v_{kij} to 0 if the average output of the surrounding eight neurons is less than 0.5.

Land-cover proportion constraint P_{kij} aims to retain the pixel class proportion output from the soft classification. For SMMI, as every sub-pixel (i.e. each neuron in the HNN), belongs to N images, the whole constraint P_{kij} will be the sum of all proportion constraints for each image:

$$P_{kij} = \sum_{n=1}^{N} L_n P_{kij}^n, \tag{6}$$

Downloaded By: [Ling, F.] At: 01:31 8 October 2010

where L_n is the weighting constant of the proportion constraint for each image. P^n_{kij} is the proportion constraint of the nth image and is defined as:

$$\frac{\mathrm{d}P^n_{kij}}{\mathrm{d}v_{kij}} = \frac{1}{2z^2} \sum_{b=xz}^{xz+z-1} \sum_{c=xz}^{yz+z-1} (1 + \tanh(v_{kbc} - 0.5)\lambda) - a^n_{kxy}, \tag{7}$$

where $1/2z^2 \sum_{b=xz}^{xz+z-1} \sum_{c=xz}^{yz+z-1} (1 + \tanh(v_{kbc} - 0.5)\lambda)$ is the estimated proportion and a^n_{kxy} is the input proportion of the land cover k of the pixel (x,y), which is the corresponding original spatial resolution pixel of the sub-pixel or neuron (k,i,j) in the nth image. z is the zoom factor, which determines the increase in spatial resolution from the original image to the super-resolution mapping image. If the area proportion estimate for class k is lower than the input proportion, a negative gradient is produced to increase the output values of neurons within the pixel (x,y) in the class layer k. Conversely, if the estimated proportion is greater than the input proportion, the proportion constraint produces a positive value to increase the output values of the neurons in the class k.

The multiclass constraint value M_{kij} aims to make the sum of classes at the position (i,j) to be equal to 1, which ensures that the outputs from each class layer have no gaps or overlaps between land-cover classes in the result. The value of the multiclass constraint is calculated as:

$$\frac{\mathrm{d}M_{kij}}{\mathrm{d}v_{kij}} = \left(\sum_{k=0}^{c} v_{kij} \right) - 1. \tag{8}$$

For super-resolution mapping, the HNN model must be initialized. Two initialization strategies can be used for the model, a random initialization and an initialization with land-cover proportion values. There are no significant differences in the results from either of the two initialization techniques (Tatem *et al.* 2001a). As the corresponding soft classification inputs are difficult to be satisfied simultaneously, all neurons are random initializations of neuron outputs within the range [0.45, 0.55] in this study.

3. Results and discussion

A set of synthetic images derived from three artificial shapes and a real QuickBird image were used to illustrate and validate the performance of the proposed SMMI technology. To avoid introducing extra error by the uncertainty of the soft classification result, these original high-resolution images were first classified to yield a high-resolution class map, and then simulated data were obtained by degrading this classification result. The area proportions of all classes in each low-resolution pixel were calculated in a window size according to the zoom factor. The corresponding fraction images were considered as the soft classification result and were then used as the inputs for the subsequent super-resolution land-cover mapping algorithm.

An additional issue concerning SMMI is the image co-registration, which is also a currently active topic in field of super-resolution reconstruction with multiple images (Park *et al.* 2003, Choi *et al.* 2004). The sub-pixel registration method is beyond the scope of this paper and many algorithms dealing with this issue can be used for this

Downloaded By: [Ling, F.] At: 01:31 8 October 2010

purpose. In this study, as the low-resolution images are all derived by degrading the fine spatial resolution maps, the sub-pixel shifts between these images are assumed to be known.

3.1 *Simulated artificial imagery*

In this experiment, three simulated artificial images were used to validate the proposed SMMI algorithm by comparing it with the traditional SMSI method. The simulated images included three types of shapes shown as figures 4(*a*), (*f*) and (*k*). All images were 56 × 56 pixels and two classes representing the shape (white) and the background (black) were considered. The zoom factor was set at 7. Thus, the simulated low-resolution images contained 8 × 8 pixels and each low-resolution pixel contained 7 × 7 pixels of the original high-resolution image. This caused mixing of the two classes at the shape boundaries, shown as figures 4(*b*), (*g*) and (*l*).

For SMMI, multiple low-resolution images with sub-pixel shifts must be used for the inputs of the HNN model. To simulate these sub-pixel shifted images, the original high-resolution image was shifted at the pixel scale in the x and y directions. The shifted image was then degraded as described previously. This procedure was performed many times according to the number of images used for SMMI. The fraction maps were calculated directly from these sub-pixel shifted images. As the shift of the original image was known, these degraded images could be accurately registered at the sub-pixel scale.

Downloaded By: [Ling, F.] At: 01:31 8 October 2010

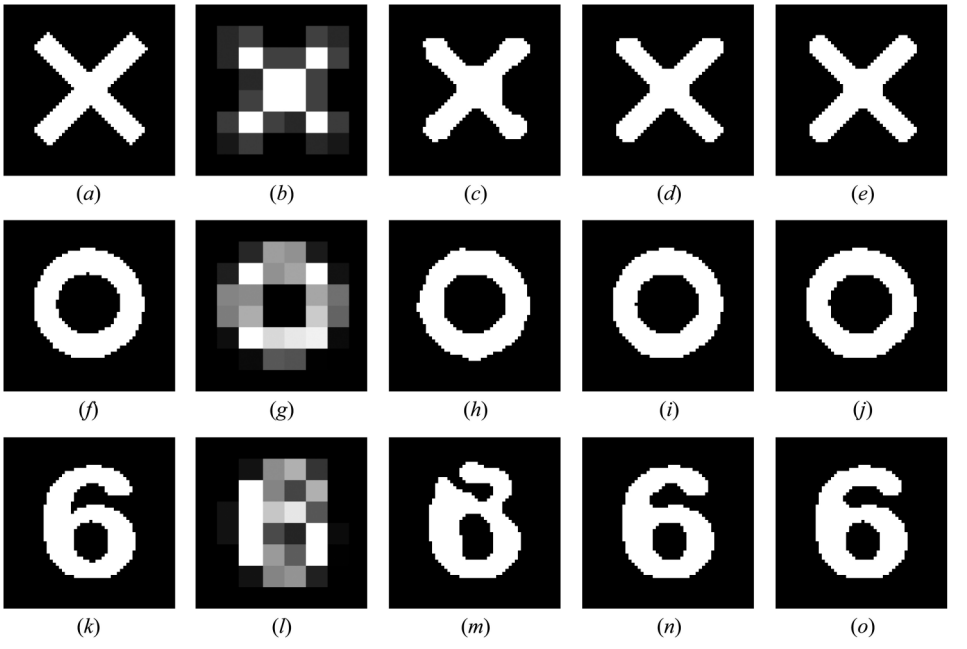

Figure 4. Simulated artificial imagery and super-resolution mapping result with single and multiple images. (*a*), (*f*) and (*k*) Three simulated artificial images (56×56 pixels). (*b*), (*g*) and (*l*) Degraded images with zoom factor z=7. (*c*), (*d*) and (*e*) Resulting map derived from (*a*) with one, four and eight images. (*h*), (*i*) and (*j*) Resulting map derived from (*f*) with one, four and eight images. (*m*), (*n*) and (*o*) Resulting map derived from (*k*) with one, four and eight images.

The HNN model was initialized by randomly setting all neurons outputs within the range [0.45, 0.55]. The constraint weighting constants $W1$, $W2$ and $W3$ were set at 1, to ensure that no single function had a dominant effect on the energy function. $C1_{kij}$ and $C2_{kij}$ always have the same effect on the spatial clustering function and they were both set at 0.5. The weighting constants L_n of the land-cover proportion constraint for each image were all set to be $1/N$, where N is the number of images. The gain or the steepness of the tanh function λ was set at 100, the time step of the iterative method dt was set at 0.01 and the iteration time was set at 5000.

As previous research has shown, the result of SMSI is more accurate than hard classification technologies (Atkinson 1997, Tatem *et al.* 2002, Mertens *et al.* 2003, Atkinson 2005, Foody *et al.* 2005). Consequently, the SMMI result was only compared with the result of SMSI for assessment of its ability to derive land-cover information at the sub-pixel scale.

Visual comparison of the results of both techniques showed that SMMI was more effective than SMSI. For the first shape shown in figure 4(*a*), the resulting maps of super-resolution mapping with one, four and eight images are shown in figures 4(*c*), (*d*) and (*e*), respectively. The SMMI maps produced by four and eight images were both more similar to the reference than was that of SMSI (super-resolution mapping with 1 image). Although there were still some minor differences between the resulting SMMI maps and the reference map, the improvement was noticeable. The right angle corners of the shape were not preserved in figure 4(*c*), while they were presented more precisely in figures 4(*d*) and (*e*). The crossover in the shape was another example that illustrated the different performance of these technologies. In figure 4(*c*), the crossover in the shape was more likely to be presented as a circle, because the spatial dependence of a circle is larger than a crossover. With an increase in the number of images, more information about the spatial distribution of the shape was incorporated into the HNN model. This zone in the resulting map was no longer a circle but became a crossover similar to that seen in the reference map. For the second and third shapes, although the improvement was different, the resulting maps of SMMI were all more similar to the reference map than was that of SMSI. This was especially true for the third shape, as the original shape was not distinguished with SMSI, while SMMI could well reconstruct the shape.

The error mapping pixels (EMP) were used as a statistical index to validate the performance of SMMI quantitatively and the results are shown in table 1. The EMPs of three shapes were much different, because the spatial pattern of the target shape has a pronounced effect on the performance of SMSI and SMMI. However, compared with SMSI, SMMI always had a considerably lower EMP index, which equates to an increase in mapping accuracy. For the first shape, EMP was 40/38 for SMSI (the first numeral is the number of the white shape pixels misclassified to a black background

Table 1. Results of error mapping pixels (EMP) for an artificial image with SMSI and SMMI. The former is the number of shape pixels misclassified to the background pixels, and the latter is the inverse.

EMP	One image	Four images	Eight images
First shape	40/38	16/10	10/6
Second shape	19/18	5/10	2/4
Third shape	71/74	12/19	8/14

Downloaded By: [Ling, F.] At: 01:31 8 October 2010

pixel and the second was the inverse). For SMMI, the EMP decreased to 16/10 for four images and 10/6 for eight images respectively, which was only about one-third and one-quarter of that seen for SMSI. A similar tendency was noted for the second and third shapes, although the decrease in EMP was not the same. The number of sub-pixel shifted images used in SMMI also influenced the performance of SMMI. When more images were used, the EMP was reduced and the super-resolution mapping had higher accuracy.

3.2 *Degraded real remotely sensed images*

To further assess the capability of the proposed SMMI technology to address a real natural phenomenon, a QuickBird image was used in this section to provide a more realistic test. The test area was located in Wuhan city, HuBei province, China. The experiment was implemented using a real panchromatic (PAN) QuickBird image of 70×70 pixels (at 0.6 m spatial resolution) shown in figure 5(*a*). According to a field investigation, the area consisted of three land-cover classes: trees, grass and roadways. The land-cover map shown in figure 5(*b*) was obtained by manually digitizing the PAN image, in which the tree class was shown as black, the grass class was shown as grey and the roadway class was shown as white.

Downloaded By: [Ling, F.] At: 01:31 8 October 2010

As was done with the simulated artificial image, the real QuickBird image was degraded to low-resolution images. Figures 5(*c*) and (*d*) show the degraded real QuickBird PAN images with zoom factors $z = 5$ and $z = 7$, respectively. The degraded low-resolution images shown here were used only for visual comparison. As it is impossible to calculate the proportion of each class through soft classification technologies only from a single PAN image, the fraction maps were extracted directly from the high-resolution land-cover image to ensure their correctness. The HNN model operation parameters were set to be the same as the previous simulated artificial images. For the SMMI technology, 4, 8 and 12 sub-pixel shifted images were used to evaluate the effect of the number of images on the super-resolution mapping result. The resulting SMSI and SMMI maps are shown in figures 5(*e*)–(*l*).

Compared with the reference high-resolution land-cover map shown in figure 5(*b*), the resulting land-cover maps produced by the SMSI technology were not visually accurate, especially for the road class and the tree class. In the reference map, the road formed a circle. However, in the resulting SMSI map, the road class became several spatially separated patches. For the tree class, small patches had almost disappeared and were combined to larger patches in the SMSI map. With an increase in the zoom factor, the patches became larger and smoother.

In comparison with SMSI, the resulting land-cover maps produced by SMMI were more accurate. The zoom factor $z = 5$ was used here to illustrate the performance of SMMI. Focusing on the road class, a great improvement was noticed. No matter how many images were used, the resulting road class never appeared as separated patches as it had with SMSI, but became a continuous circle similar to the reference map, although there were still some minor differences between these maps and the reference map. For the tree class, as more images were used for SMMI, the result became more precise, especially for the location and shape of patches. For SMMI with four images, small patches at the north-east corner were still not represented at accurate locations in the resulting map and several central small patches were combined to form a large patch. However, with 12 images, the shapes and locations were represented more accurately and became much more similar to those in the reference map.

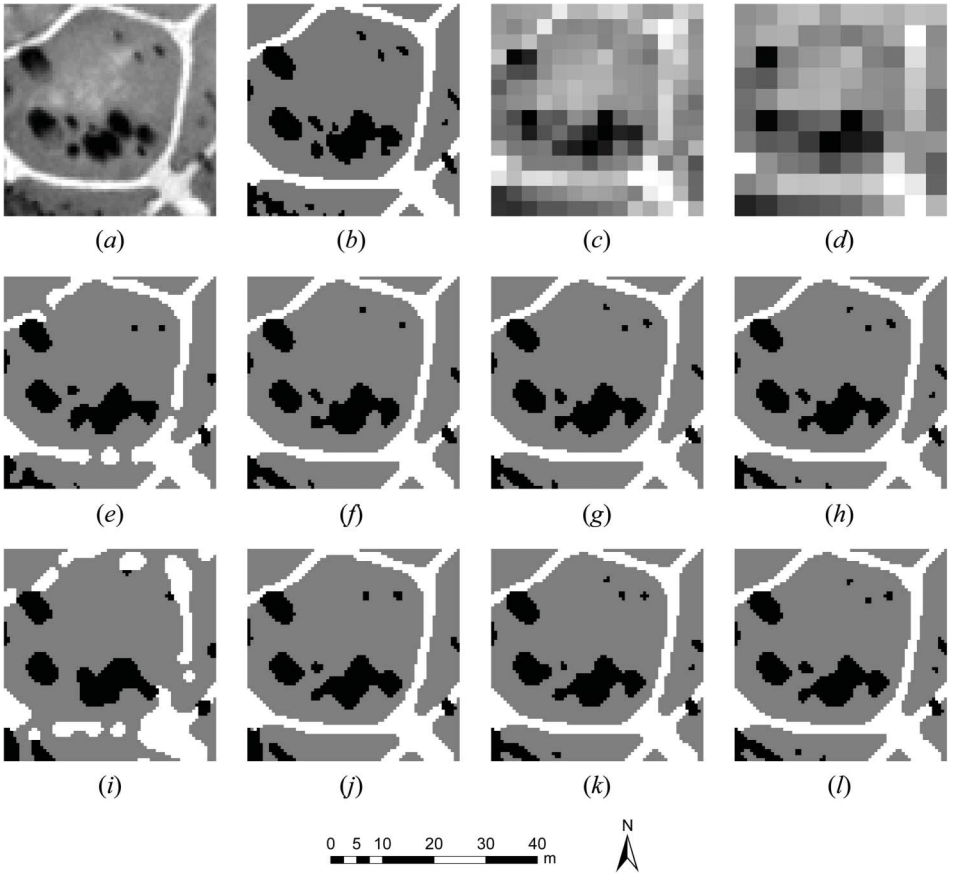

Figure 5. Degraded real QuickBird imagery and super-resolution mapping result with single and multiple images. (*a*) QuickBird 0.6-m panchromatic image (70×70 pixels) with the central point located at 30°35′50.9″N and 114°19′55.8″E; (*b*) land-cover class image (black represents trees, grey is grass, and white is roadways); (*c*) degraded image with zoom factor z=5; (*d*) degraded image with zoom factor z=7; (*e*), (*f*), (*g*) and (*h*) resulting super-resolution mapping images derived from 1, 4, 8 and 12 images at zoom factor 5; (*i*), (*j*), (*k*) and (*l*) resulting super-resolution mapping images derived from 1, 4, 8 and 12 images at zoom factor 7.

The accuracy statistics showed a considerable increase in accuracy with the proposed SMMI technology (table 2). For the zoom factor $z = 5$, overall accuracy increased from 93.65% for SMSI to 97.79%, 98.21% and 98.85% for SMMI with 4, 8 and 12 images, respectively. The Kappa coefficient increased from 86.13% for SMSI to 95.21%, 96.11 and 97.52% for SMMI with 4, 8 and 12 images. With four images, the accuracy had an improvement of 4.14% in terms of overall accuracy and 9.08% for the Kappa coefficient. Although more images were used for SMMI, the result was more accurate; there was only about a 1% increase in overall accuracy and the Kappa coefficient by adding four images, step by step. A similar trend was also noticed for the zoom factor $z = 7$. Compared with SMSI, the overall accuracy of SMMI with four images increased about 10% and the Kappa coefficient increased about 25%. Although the resulting map was more accurate with the increase in image number, the result accuracy had no distinct improvement and an increase of only about 1% could be achieved by adding four more images.

Downloaded By: [Ling, F.] At: 01:31 8 October 2010

Table 2. Results of accuracy analysis for a real QuickBird image with SMSI and SMMI at different zoom factors.

Statistics index	Overall accuracy (%)		Kappa coefficient (%)	
Scale factor	$z = 5$	$z = 7$	$z = 5$	$z = 7$
One image	93.65	85.28	86.13	67.92
Four images	97.79	95.81	95.21	91.91
Eight images	98.21	96.97	96.11	93.00
Twelve images	98.85	98.47	97.52	94.52

4. Conclusions

Super-resolution mapping is a post processing technology of soft classification used to predict spatial land-cover patterns at the sub-pixel scale. Although this can provide a more informative representation than the result of soft classification, SMSI always has uncertainty; the fraction maps derived from only one image cannot provide enough information about the land-cover distribution at the sub-pixel scale. However, as satellites always have multiobservation capability, multiple sub-pixel shifted images can be used to provide more useful information for super-resolution land-cover mapping.

This paper introduces the technology of super-resolution land-cover mapping using multiple sub-pixel shifted remotely sensed images. The basic principle of the proposed method is similar to that of the traditional 'super-resolution construction' method, however, both methods are essentially different. The 'super-resolution construction' method first recovers the high-resolution image and then obtains the resulting high-resolution land-cover map through a hard classification method applied to the reconstructed image. In contrast, the proposed method first derives the fraction maps of each low-resolution image with a soft classification method and then combines these fraction maps to predict the resulting high-resolution land-cover map.

Compared with the 'super-resolution reconstruction' method, the input of the proposed method is not the images themselves but the fraction maps derived from each image with soft classification technologies. Because of this, the different atmospheric conditions should not affect analysis and the atmospheric correction procedures can be ignored for most situations. Moreover, remotely sensed images with similar spatial resolution from different satellite platforms can be used together as the inputs of SMMI, and this feature extends information fusion of remotely sensed imagery.

An HNN optimization model was constructed to address the problems of SMMI. The effectiveness of the method was assessed using simulated artificial images as well as a degraded real QuickBird image. When the resulting maps derived with SMMI were compared visually and quantitatively with that derived with SMSI, for all examples, SMMI was found to achieve more precise high-resolution land-cover maps than SMSI. The results demonstrated the usefulness of the proposed SMMI technology and the HNN model.

Although the proposed SMMI technology showed good performance, there are still several issues that need to be further studied. As the simulated results in this

Downloaded By: [Ling, F.] At: 01:31 8 October 2010

research were obtained under ideal conditions without any extra errors, the uncertainty caused by soft classification and registration of multiple images needs to be investigated in more depth. An integrated model incorporating simultaneous soft classification, image registration and land-cover mapping appears to be a promising method for improvement of the SMMI technology for practical applications.

Acknowledgements

This work was funded by the National Natural Science Foundation of China (No. 40801186, No. 40801045) and Wuhan Youth Chenguang Project (No.200950431218). The authors would like to thank the reviewers for providing constructive comments.

References

Aplin, P. and Atkinson, P.M., 2001, Sub-pixel land cover mapping for per-field classification. *International Journal of Remote Sensing*, **22**, pp. 2853–2858.

Atkinson, P.M., 1997, Mapping sub-pixel boundaries from remotely sensed images. In *Innovations in GIS 4*, pp. 166–180 (London: Taylor & Francis).

Atkinson, P.M., 2005, Sub-pixel target mapping from soft-classified, remotely sensed imagery. *Photogrammetric Engineering and Remote Sensing*, **71**, pp. 839–846.

Atkinson, P.M., Cutler, M.E.J. and Lewis, H., 1997, Mapping sub-pixel proportional land cover with AVHRR imagery. *International Journal of Remote Sensing*, **18**, pp. 917–935.

Atkinson, P.M., Pardo-Iguzquiza, E. and Chica-Olmo, M., 2008, Downscaling cokriging for super-resolution mapping of continua in remotely sensed images. *IEEE Transactions on Geoscience and Remote Sensing*, **46**, pp. 573–580.

Bastin, L., 1997, Comparison of fuzzy c-means classification, linear mixture modelling and MLC probabilities as tools for unmixing coarse pixels. *International Journal of Remote Sensing*, **18**, pp. 3629–3648.

Bonnett, R. and Campbell, J.B., 2002, *Introduction to Remote Sensing* (New York: Taylor & Francis).

Boucher, A. and Kyriakidis, P.C., 2007, Integrating fine scale information in super-resolution land-cover mapping. *Photogrammetric Engineering and Remote Sensing*, **73**, pp. 913–921.

Brown, M., Lewis, H.G. and Gunn, S.R., 2000, Linear spectral mixture models and support vector machines for remote sensing. *IEEE Transactions on Geoscience and Remote Sensing*, **38**, pp. 2346–2360.

Carpenter, G.A., Gopal, S., Macomber, S., Martens, S. and Woodcock, C.E., 1999, A neural network method for mixture estimation for vegetation mapping. *Remote Sensing of Environment*, **70**, pp. 138–152.

Choi, E., Choi, J. and Kang, M.G., 2004, Super-resolution approach to overcome physical limitations of imaging sensors: An overview. *International Journal of Imaging Systems and Technology*, **14**, pp. 36–46.

Cracknell, A.P., 1998, Synergy in remote sensing – what's in a pixel? *International Journal of Remote Sensing*, **19**, pp. 2025–2047.

Elad, M. and Feuer, A., 1999, Superresolution restoration of an image sequence: Adaptive filtering approach. *IEEE Transactions on Image Processing*, **8**, pp. 387–395.

Fisher, P., 1997, The pixel: A snare and a delusion. *International Journal of Remote Sensing*, **18**, pp. 679–685.

Foody, G.M., 1996, Approaches for the production and evaluation of fuzzy land cover classifications from remotely-sensed data. *International Journal of Remote Sensing*, **17**, pp. 1317–1340.

Foody, G.M., 1998, Sharpening fuzzy classification output to refine the representation of sub-pixel land cover distribution. *International Journal of Remote Sensing*, **19**, pp. 2593–2599.

Downloaded By: [Ling, F.] At: 01:31 8 October 2010

Foody, G.M., 2002, Hard and soft classifications by a neural network with a non-exhaustively defined set of classes. *International Journal of Remote Sensing*, **23**, pp. 3853–3864.

Foody, G.M., Muslim, A.M. and Atkinson, P.M., 2005, Super-resolution mapping of the waterline from remotely sensed data. *International Journal of Remote Sensing*, **26**, pp. 5381–5392.

Friedl, M.A., McIver, D.K., Hodges, J.C.F., Zhang, X.Y., Muchoney, D., Strahler, A.H., Woodcock, C.E., Gopal, S., Schneider, A., Cooper, A., Baccini, A., Gao, F. and Schaaf, C., 2002, Global land cover mapping from MODIS: algorithms and early results. *Remote Sensing of Environment*, **83**, pp. 287–302.

GarciaHaro, F.J., Gilabert, M.A. and Melia, J., 1996, Linear spectral mixture modelling to estimate vegetation amount from optical spectral data. *International Journal of Remote Sensing*, 17, pp. 3373–3400.

Hardie, R.C., Barnard, K.J. and Armstrong, E.E., 1997, Joint MAP registration and high-resolution image estimation using a sequence of undersampled images. *IEEE Transactions on Image Processing*, 6, pp. 1621–1633.

Holben, B.N. and Shimabukuro, Y.E., 1993, Linear mixing model applied to coarse spatial-resolution data from multispectral satellite sensors. *International Journal of Remote Sensing*, **14**, pp. 2231–2240.

Hung, M.C. and Ridd, M.K., 2002, A subpixel classifier for urban land-cover mapping based on a maximum-likelihood approach and expert system rules. *Photogrammetric Engineering and Remote Sensing*, **68**, pp. 1173–1180.

Irani, M. and Peleg, S., 1991, Improving resolution by image registration. In *CVGIP: Graphical Models and Image Processing*, pp. 231–239.

Kasetkasem, T., Arora, M.K. and Varshney, P.K., 2005, Super-resolution land cover mapping using a Markov random field based approach. *Remote Sensing of Environment*, **96**, pp. 302–314.

Kim, S.P. and Su, W.Y., 1993, Recursive high-resolution reconstruction of blurred multiframe images. *IEEE Transactions on Image Processing*, **2**, pp. 534–539.

Lee, S. and Lathrop, R.G., 2006, Subpixel analysis of Landsat ETM+ using Self-Organizing Map (SOM) neural networks for urban land cover characterization. *IEEE Transactions on Geoscience and Remote Sensing*, **44**, pp. 1642–1654.

Ling, F., Xiao, F., Du, Y., Xue, H.P. and Ren, X.Y., 2008, Waterline mapping at the subpixel scale from remote sensing imagery with high-resolution digital elevation models. *International Journal of Remote Sensing*, **29**, pp. 1809–1815.

Liu, W.G., Seto, K.C., Wu, E.Y., Gopal, S. and Woodcock, C.E., 2004, ART-MMAP: A neural network approach to subpixel classification. *IEEE Transactions on Geoscience and Remote Sensing*, **42**, pp. 1976–1983.

Liu, W.G. and Wu, E.Y., 2005, Comparison of non-linear mixture models: Sub-pixel classification. *Remote Sensing of Environment*, **94**, pp. 145–154.

Loveland, T.R., Reed, B.C., Brown, J.F., Ohlen, D.O., Zhu, Z., Yang, L. and Merchant, J.W., 2000, Development of a global land cover characteristics database and IGBP DISCover from 1 km AVHRR data. *International Journal of Remote Sensing*, **21**, pp. 1303–1330.

Lu, Y. and Inamura, M., 2003, Spatial resolution improvement of remote sensing images by fusion of subpixel-shifted multi-observation images. *International Journal of Remote Sensing*, **24**, pp. 4647–4660.

Makido, Y., Shortridge, A. and Messina, J.P., 2007, Assessing alternatives for modeling the spatial distribution of multiple land-cover classes at sub-pixel scales. *Photogrammetric Engineering and Remote Sensing*, **73**, pp. 935–943.

Maltamo, M., Tokola, T. and Lehikoinen, M., 2003, Estimating stand characteristics by combining single tree pattern recognition of digital video imagery and a theoretical diameter distribution model. *Forest Science*, **49**, pp. 98–109.

Downloaded By: [Ling, F.] At: 01:31 8 October 2010

MERTENS, K.C., VERBEKE, L.P.C., DUCHEYNE, E.I. and DE WULF, R.R., 2003, Using genetic algorithms in sub-pixel mapping. *International Journal of Remote Sensing*, **24**, pp. 4241–4247.

MERTENS, K.C., VERBEKE, L.P.C., WESTRA, T. and DE WULF, R.R., 2004, Sub-pixel mapping and sub-pixel sharpening using neural network predicted wavelet coefficients. *Remote Sensing of Environment*, **91**, pp. 225–236.

NGUYEN, M.Q., ATKINSON, P.M. and LEWIS, H.G., 2005, Super resolution mapping using a Hopfield neural network with LIDAR data. *IEEE Geoscience and Remote Sensing Letters*, **2**, pp. 366–370.

NGUYEN, M.Q., ATKINSON, P.M. and LEWIS, H.G., 2006, Super resolution mapping using a hopfield neural network with fused images. *IEEE Transactions on Geoscience and Remote Sensing*, **44**, pp. 736–749.

PACKALEN, P., TOKOLA, T., SAASTAMOINEN, J. and MALTAMO, M., 2006, Use of a super-resolution method in interpretation of forests from multiple NOAA/AVHRR images. *International Journal of Remote Sensing*, **27**, pp. 5341–5357.

PARK, S.C., PARK, M.K. and KANG, M.G., 2003, Super-resolution image reconstruction: A technical overview. *IEEE Signal Processing Magazine*, **20**, pp. 21–36.

ROBIN, A., LE HEGARAT-MASCLE, S. and MOISAN, L., 2008, Unsupervised subpixelic classification using coarse-resolution time series and structural information. *IEEE Transactions on Geoscience and Remote Sensing*, **46**, pp. 1359–1374.

SAWAYA, K.E., OLMANSON, L.G., HEINERT, N.J., BREZONIK, P.L. and BAUER, M.E., 2003, Extending satellite remote sensing to local scales: land and water resource monitoring using high-resolution imagery. *Remote Sensing of Environment*, **88**, pp. 144–156.

SEAN, B. and ROBERT, L.S., 1998, Super-resolution from image sequences – a review. In *Proceedings of the 1998 Midwest Symposium on Systems and Circuits*, Notre Dame, IN, USA (Piscataway, NJ: IEEE Computer Society), pp. 374–378.

SONG, C., WOODCOCK, C.E., SETO, K.C., LENNEY, M.P. and MACOMBER, S.A., 2001, Classification and change detection using Landsat TM data: When and how to correct atmospheric effects? *Remote Sensing of Environment*, **75**, pp. 230–244.

STARK, H. and OSKOUI, P., 1989, High-resolution image recovery from image-plane arrays using convex projections. *Journal of the Optical Society of America*, **6**, pp. 1715–1726.

TATEM, A.J., LEWIS, H.G., ATKINSON, P.M. and NIXON, M.S., 2001a, Super-resolution target identification from remotely sensed images using a Hopfield neural network. *IEEE Transactions on Geoscience and Remote Sensing*, **39**, pp. 781–796.

TATEM, A.J., LEWIS, H.G., ATKINSON, P.M. and NIXON, M.S., 2001b, Multiple-class land-cover mapping at the sub-pixel scale using a Hopfield neural network. *International Journal of Applied Earth Observation and Geoinformation*, **3**, pp. 184–190.

TATEM, A.J., LEWIS, H.G., ATKINSON, P.M. and NIXON, M.S., 2002, Super-resolution land cover pattern prediction using a Hopfield neural network. *Remote Sensing of Environment*, **79**, pp. 1–14.

TATEM, A.J., LEWIS, H.G., ATKINSON, P.M. and NIXON, M.S., 2003, Increasing the spatial resolution of agricultural land cover maps using a Hopfield neural network. *International Journal of Geographical Information Science*, **17**, pp. 647–672.

THORNTON, M.W., ATKINSON, P.M. and HOLLAND, D.A., 2007, A linearised pixel-swapping method for mapping rural linear land cover features from fine spatial resolution remotely sensed imagery. *Computers & Geosciences*, **33**, pp. 1261–1272.

TSAI, R.Y. and HUANG, T.S., 1984, Multipleframe image restoration and registration. In *Advances in Computer Vision and Image Processing*, pp. 317–339 (Greenwich, CT: JAI Press).

VERHOEYE, J. and DE WULF, R., 2002, Land cover mapping at sub-pixel scales using linear optimization techniques. *Remote Sensing of Environment*, **79**, pp. 96–104.

Downloaded By: [Ling, F.] At: 01:31 8 October 2010